[Prepared for publication as an Article in *J. Phys. Chem. B*.]

Single-Molecule Tracking Study of the Permeability and Transverse Width of Individual Cylindrical Microdomains in Solvent-Swollen Polystyrene-*block*-Poly(ethylene oxide) Films

Dol Raj Sapkota, Khanh-Hoa Tran-Ba,[†] Trevor Elwell-Cuddy, Daniel A. Higgins,* and Takashi Ito*

Department of Chemistry, Kansas State University, 213 CBC Building, Manhattan, Kansas 66506-0401, USA

[†] Present Address: Department of Chemistry, Columbia University, New York, NY 10027, USA

* To whom correspondence should be addressed.

Email: ito@ksu.edu (T.I.); higgins@ksu.edu (D.A.H.)

Telephone: 785-532-1451 (T.I.); 785-532-6371 (D.A.H.)

Fax: 785-532-6666 (T.I.); 785-532-6666 (D.A.H.)

Abstract

Understanding the properties of solvent-swollen block copolymer (BCP) microdomains is important for better solvent-based control of microdomain morphology, orientation and permeability. In this study, single-molecule tracking (SMT) was explored to assess the permeability and transverse width of individual cylindrical microdomains in solvent-swollen polystyrene-*block*-poly(ethylene oxide) (PS-*b*-PEO) films. PS-*b*-PEO films comprising shear-elongated cylindrical PEO microdomains were prepared by sandwiching its benzene or tetrahydrofuran (THF) solution between two glass substrates. SMT measurements were performed at different drying times to investigate the effects of solvent evaporation on the microdomain properties. SMT data showed one-dimensional (1D) motions of single fluorescent molecules (sulforhodamine B) based on their diffusion within the cylindrical microdomains. Microdomain permeability and transverse width were assessed from the single-molecule diffusion coefficients (D_{SMT}) and transverse variance of the 1D trajectories (σ_δ^2), respectively. The D_{SMT} and σ_δ^2 values from individual 1D trajectories were widely distributed with no evidence of correlation on a single molecule basis, possibly because the individual microdomains in a film were swollen to different extents. On average, microdomain permeability (D) and effective radius (r) gradually decreased within the first three days of drying due to solvent evaporation, and changed negligibly thereafter. PS-*b*-PEO films prepared from THF solutions exhibited larger changes in D and r as compared with those from benzene solutions due to the better swelling of the PEO microdomains by THF. Importantly, changes in D were more prominent than those in r, suggesting that the permeability of the PEO microdomains is very susceptible to the presence of solvent. These results reveal the unique capability of SMT to assess the properties of individual cylindrical microdomains in a solvent-swollen BCP film.

Introduction

Block copolymers (BCPs) are constructed from covalently-linked homopolymers based on distinct chemical compositions.[1,2] These polymers can afford self-organized nanostructures (microdomains) with dimensions and morphologies that are predictable from their thermodynamic compatibility and molecular weights.[1,3] Among the morphologies that can be obtained from BCPs, cylindrical morphologies have attracted considerable interest due to their wide applicability as lithographic masks,[4,5] templates for nanomaterial synthesis,[4] chemical separation and sensing media,[6-8] and model polyelectrolytes for fuel cells and batteries.[9,10] For these applications, cylindrical microdomains in thin monolithic films/membranes need to be aligned in a desired direction. A number of methods for aligning the microdomains have been explored, including those based on mechanical flow fields, temperature gradients, electric fields and solvent control.[3,11,12]

Among these methods, solvent-based methods such as solvent vapor annealing (SVA)[13] have been recognized as effective means to obtain BCP films/membranes with controlled morphologies because they can quickly offer well-controlled nanostructures over a large area. In SVA[14-16] and related methods such as solvent vapor penetration,[17,18] individual BCP segments are first swollen by solvent vapor to different extents according to the solvent-segment compatibilities. Solvent swelling enhances the flexibility of the polymer chains, resulting in the facilitated rearrangement of microdomains during subsequent solvent evaporation. The resulting microdomain morphology and alignment are affected by the solvent evaporation rate and direction[14-16] as well as solvent-segment compatibility.[16,18-21] The morphologies and dimensions of these microdomains were often measured for completely dried samples[14-16] using scanning probe microscopy[22,23] and electron microscopy,[24] but these microscopic methods are difficult to

use for *in situ* measurements of solvent-swollen samples. More recently, real-time grazing-incidence small-angle X-ray scattering (GISAXS) has been employed to gain insight into the roles of solvent(s) during their evaporation in determining microdomain orientation and spacing.[16,25-28] Although offering valuable information on microdomain morphologies and spacing for different solvent contents, GISAXS only provides spatially- and temporarily-averaged information from periodic structures. Meanwhile, recent computational studies have been explored to understand the roles of solvent in the solvent-based methods, including the effects of solvent-polymer compatibility and solvent evaporation rate on the microdomain orientation.[29,30]

In this study, single-molecule tracking (SMT) was employed to characterize the properties of elongated cylindrical microdomains in polystyrene-*block*-poly(ethylene oxide) (PS-*b*-PEO; **Figure 1a**) thin films. SMT measures the motions of individual fluorescent molecules using wide-field fluorescence microscopy.[31-35] A PS-*b*-PEO thin film comprising elongated cylindrical PEO microdomains in a PS matrix was prepared by sandwiching a concentrated PS-*b*-PEO solution between a glass coverslip and a glass slide. PEO microdomain elongation was based on shear flow (**Figure 1b**).[36] In addition, the two glass substrates restricted solvent evaporation to the horizontal direction (*i.e.*, the observation plane), preventing the microdomains from orienting perpendicularly to the substrate surface. Diffusional motions of individual sulforhodamine B (SRB; **Figure 1a**) molecules doped into the cylindrical microdomains were recorded as a function of drying time. The resulting single-molecule trajectories were analyzed using orthogonal regression methods[37] to assess the microdomain permeability and transverse width. Cylinder-forming PS-*b*-PEO was studied for the following reasons. First, it has been shown that the orientation of its cylindrical PEO microdomains can be tuned via solvent-based methods.[16,18]

Thus, *in situ* characterization of solvent-swollen PS-*b*-PEO films will offer valuable information on the role of solvent in these methods. Second, the lateral width and molecular permeability of individual cylindrical PEO microdomains can be directly determined from the diffusional motions of PEO-selective fluorescent molecules using SMT.[18,36,38] Single molecules diffusing in elongated cylindrical microdomains yield one-dimensional (1D) trajectories, and thus can be selectively recognized. It should be noted that SMT was used previously to investigate microdomain alignment[18,36,38] and to compare single-molecule and ensemble diffusion[38] in PS-*b*-PEO films dried under optimized conditions, but has not been employed to characterize microdomain properties swollen to different extents. Furthermore, monolithic PS-*b*-PEO films/membranes have been used as lithographic masks,[39] templates for nanomaterial synthesis,[40] model nanostructured polyelectrolytes for battery and fuel cell applications,[9,10] and water purification membranes.[41-43] The latter three applications involve molecular/ionic transport through the PEO microdomains, and thus information on microdomain permeability and transverse width will permit the performances of these materials to be better controlled.

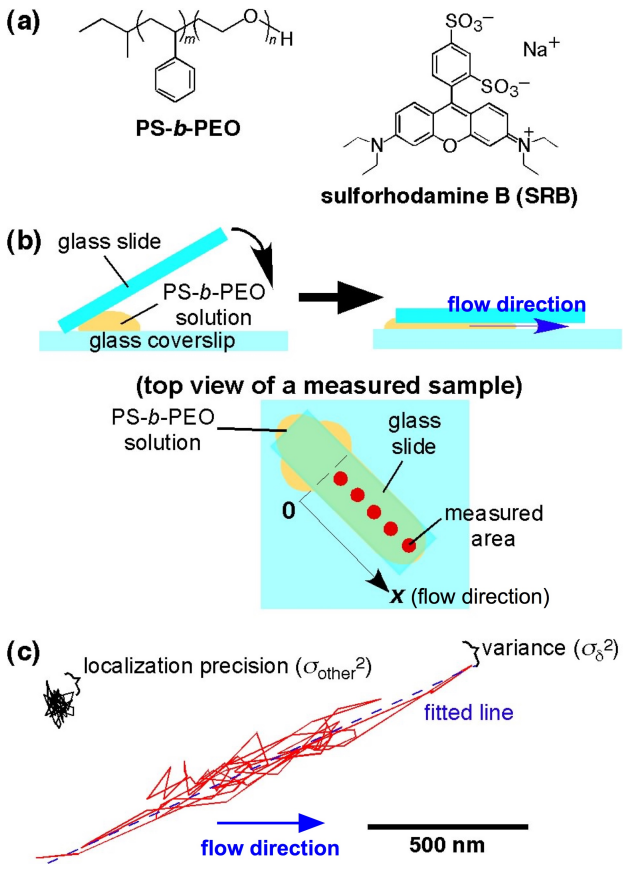

Figure 1. (a) Chemical structures of PS-*b*-PEO and sulforhodamine B (SRB). (b) Schematic illustration of the sample preparation procedure. A droplet of PS-*b*-PEO solution (25 wt%, 50 μL) was placed on a glass coverslip, and then was sandwiched by a rectangular glass slide to have the solution flow through the gap between the two glass substrates. After drying, the film was used for SMT measurements at several different in-plane positions along the flow direction, as examplified by red dots in the bottom scheme. (c) Typical 1D (red) and immobile (black) trajectories measured in a PS-*b*-PEO film prepared from THF solution upon drying for 1 day. The 1D trajectory was fitted to a line using the orthogonal regression method, and its transverse variance (σ_δ^2) was determined. Localization precision in SMT data was calculated as the average of the variances of immobile trajectories (σ_{other}^2).

Experimental Procedures

Chemicals and Materials. PS-*b*-PEO (PS, M_n = 35 000 g/mol; PEO, M_n = 10 500 g/mol; PS volume fraction 0.8; M_w/M_n = 1.10) was purchased from Polymer Source and used as received. Benzene (HPLC grade); tetrahydrofuran (THF; HPLC grade); methanol (MeOH;

HPLC grade) and SRB (ACS grade) were purchased from Acros Organics and used without further purification. A glass coverslip (FisherFinest Premium; 25 × 25 mm^2, 0.2 mm thick) was employed as a bottom substrate. A rectangular top piece was prepared from a thinner glass coverslip (Goldseal® cover glass; 22×7 mm^2, 0.1 mm thick).

Sample Preparation. A SRB-doped PS-*b*-PEO film sandwiched between a glass coverslip and a rectangular glass substrate was prepared in a nitrogen-filled glovebox (relative humidity < 20%) according to the previously reported procedure.[36] Briefly, a droplet of a PS-*b*-PEO solution (25 wt%, 50 μL) in benzene, THF, 86% benzene + 14% MeOH or 86% THF + 14% MeOH containing nominally 5 nM SRB (in the PEO microdomains) was placed on a glass coverslip. A rectangular top piece was immediately placed on the droplet to induce solution flow between the two glass substrates (**Figure 1b**). The resulting film was dried at 30 °C or 40 °C in the glovebox. SMT measurements were carried out approximately every 24 h of drying up to 96 or 120 h (4 or 5 days).

SMT Measurements. All the SMT data were recorded on a wide-field fluorescence microscope in a pseudo total internal reflection fluorescence (p-TIRF) mode, as described previously.[18,36-38] The microscope was built on an inverted epi-illumination microscope (Nikon Eclipse Ti). Light emitted by a Nd:YVO_4 laser (532 nm, 5 mW) was introduced to the back aperture of an oil-immersion objective (Nikon Apo TIRF 100X; 1.49NA) by reflection from a dichroic beam splitter (Chroma, 555 DCLP). The emitted fluorescence was collected by the objective and directed through the dichroic mirror and a bandpass–filter (Chroma, 580/40 HQ), before hitting the photosensitive surface of a back-illuminated electron-multiplying CCD camera

(Andor iXon DU-897). All SMT videos (16 × 16 μm^2 film regions; 128 pixels × 128 pixels (2 × 2 binning; 1 pixel = 125 nm)) were 1000~2000 frames in length, with a cycle time of 41 msec per frame, an electron-multiplying gain of 30, and a readout rate of 10 MHz. All SMT video data were recorded near the film–coverslip interface ($z \approx 1$ μm) at five different positions along the longitudinal direction of the rectangular piece (**Figure 1b**, bottom).

The SMT data were analyzed after generating single-molecule trajectories according to procedures reported previously.[18,36-38] Detection of fluorescent spots present in the video frame and their linking into trajectories were done by using ImageJ particle tracker software. In this study, single molecule trajectories > 10 consecutive frames in length were analyzed using orthogonal regression methods that involve fitting of individual trajectories to a straight line.[37] 1D, 2D and immobile trajectories from 1D-diffusing, 2D-diffusing and immobile molecules were classified from the variances of molecular motion along (σ_R^2) and across (σ_δ^2) each trajectory (**Figure 1c**).[37] The threshold variances were chosen at 75% confidence for the immobile trajectories obtained from Monte Carlo computer simulations. Specifically, trajectories with $\sigma_\delta > 40$ nm, those with $\sigma_\delta \leq 40$ nm and $\sigma_R \geq 77$ nm, and those with $\sigma_\delta \leq 40$ nm and $\sigma_R < 77$ nm were classified as 2D, 1D, and immobile, respectively. It should be noted that the influences of t_{dry} and solvent on the relative populations of 1D/2D/immobile trajectories were unclear for the PS-*b*-PEO films prepared in this study. 1D and immobile trajectories, as shown in **Figure 1c**, were further analyzed to gain information on the permeability and transverse width of cylindrical microdomains. These properties were assessed as the single-molecule diffusion coefficient (D_{SMT}) and σ_δ^2 from individual 1D trajectories. It should be noted that the radii of individual cylindrical microdomains can be determined if localization precision is constant. However, due to the statistical distribution of position errors and the different S/N ratios of individual videos,

the effective microdomain radius could be obtained only as an ensemble average for all the 1D trajectories in each video. Indeed, $\langle\sigma_{other}^2\rangle$ varied in the range of 150-1200 nm^2. Thus, effective microdomain radius (r) was calculated as an ensemble parameter for each video from the averages of σ_δ^2 of 1D trajectories, $\langle\sigma_\delta^2\rangle$, and position errors of immobile trajectories, $\langle\sigma_{other}^2\rangle$, using Eq (1):[18]

$$\langle\sigma_\delta^2\rangle = \langle\sigma_{other}^2\rangle + r^2 \qquad (1)$$

D_{SMT} was calculated from the mean square displacement (MSD) as a function of lag time (τ) using Eq (2) for 1D-diffusing molecules:[35,38]

$$\text{MSD}(\tau) = 2D_{SMT}\tau \qquad (2)$$

The 1D trajectories obtained in this study were not always well-aligned to the solution flow direction in contrast to our previous study.[36] The poorer alignment is possibly due to the lower solution viscosity afforded by the smaller PS-*b*-PEO (M_n(PS) = 35,000 and M_n(PEO) = 10,500 used in this study; M_n(PS) = 42,000 and M_n(PEO) = 11,500 in the previous study) at the lower concentration (25 wt% in this study; 30 wt% in the previous study). The inconsistent microdomain alignment was observed for PS-*b*-PEO films regardless of solution composition. In addition, technical difficulties prevented the monitoring of identical microdomains at different t_{dry}. Thus, the microdomain alignment was not discussed in this study.

Results and Discussion

In this study, SMT measurements were carried out for solvent-swollen, SRB-doped PS-*b*-PEO films after different drying times (t_{dry}). SRB molecules selectively partitioned into the PEO microdomains, and thus provided information on the properties of individual PEO

microdomains.[18] 1D trajectories from SRB molecules in SMT videos were analyzed to quantitatively assess the permeabilities and transverse widths of individual cylindrical PEO microdomains. Different solvents were employed for the preparation of PS-*b*-PEO precursor solutions to investigate the effects of solvent-segment compatibilities on the microdomain properties in the wet films. **Table 1** summarizes the Hansen solubility parameters of polymers and solvents used in this study.[44,45] Benzene and THF were examined as solvents for the following three reasons. First, these solvents can dissolve PS-*b*-PEO to give uniform solutions. Second, they are fairly volatile (boiling points: 66.0 °C for THF and 80.1 °C for benzene)[46] so that the samples can be gradually dried at relatively low temperature (30 or 40 °C) over a relatively short period of time. Most importantly, these two solvents have different compatibilities with PS and PEO, as suggested by the *Ra* values in the table: Benzene selectively swells PS, while THF is slightly selective for PEO. Benzene and THF are both important solvents that have been used for solvent annealing experiments in several block copolymer systems including PS-*b*-PEO.[16,47] In addition, the effects of MeOH addition to PS-*b*-PEO solutions were investigated, because MeOH (boiling point: 64.7 °C)[46] is known to swell PEO[48] in spite of its large *Ra* value in **Table 1**. Measurements at different t_{dry} with different solvents will provide a means to investigate the influence of polymer deswelling induced by solvent evaporation on the microdomain properties.

Table 1. Solubility Parameters[a)] and Compatibility of Polymer Segments and Solvents/Solutions Used in This Study

(i) Polymer Segments

polymer	δ(D)[b)]	δ(P)[c)]	δ(H)[d)]
PS	18.5	4.5	2.9
PEO	17	10	5

(ii) Solvents

solvent	δ(D)[b)]	δ(P)[c)]	δ(H)[d)]	*Ra* (PS)[e)]	*Ra* (PEO)[e)]
benzene	18.4	0	2	4.6	10.8
THF	16.8	5.7	8	6.2	5.3
methanol	15.1	12.3	22.3	22.0	17.9

[a)] Taken from literature.[44,45] [b)] Dispersion component. [c)] Polar component. [d)] Hydrogen bonding component. [e)] Calculated using the following equation: $Ra^2 = 4\left(\delta_{D,polymer} - \delta_{D,solvent}\right)^2 + \left(\delta_{P,polymer} - \delta_{P,solvent}\right)^2 + \left(\delta_{H,polymer} - \delta_{H,solvent}\right)^2$. *Ra* < 8 for good solvent.[44,45]

Figure 2a shows typical 1D, 2D and immobile trajectories obtained in a PS-*b*-PEO film prepared from its benzene solution and dried at 40 °C for t_{dry} = 1, 3 and 5 days. A number of 1D trajectories, attributable to single SRB molecules diffusing within elongated cylindrical PEO microdomains, were observed in each of these data. **Figure 2b** shows the relationship between the D_{SMT} and σ_δ^2 values of these individual 1D trajectories. Both D_{SMT} and σ_δ^2 seemed to slightly decrease at longer t_{dry}, probably due to the deswelling of cylindrical PEO microdomains as a result of solvent evaporation. However, these parameters exhibited wide distributions regardless of t_{dry}, suggesting that the individual PEO microdomains were swollen to different extents, possibly due to non-uniform solvent evaporation from microdomains of different solvent compatibilities. In addition, no evidence of correlation between D_{SMT} and σ_δ^2 was observed in contrast to hindered diffusion within solid pores that exhibits slower diffusion in smaller pores.[49] The absence of a correlation suggests that the PEO microdomains were too large as compared

with SRB molecules to attain hindered diffusion.

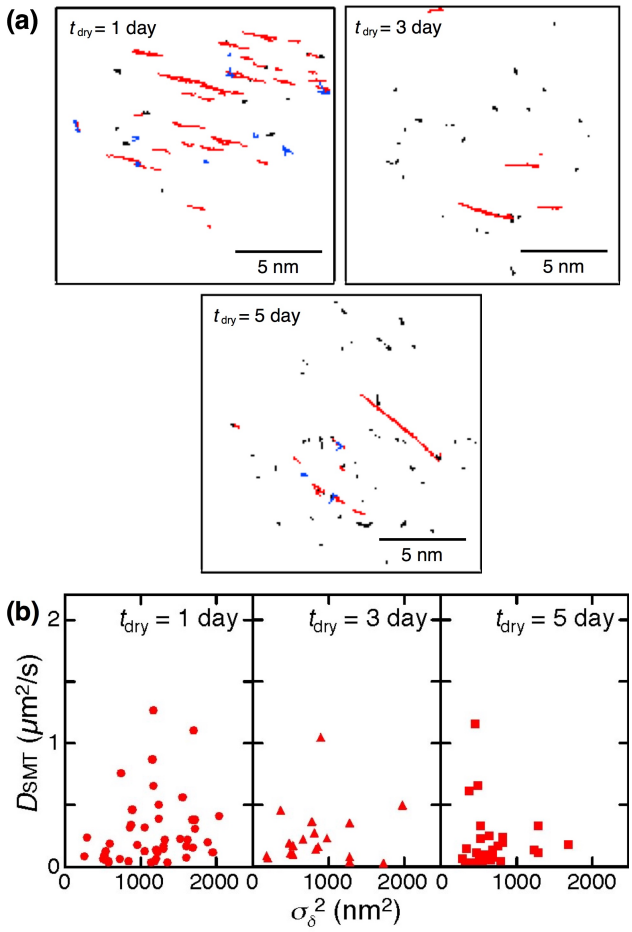

Figure 2. (a) Representative single-molecule trajectories > 10 consecutive frames in length that were measured in a PS-*b*-PEO film prepared from a benzene solution (25 wt%) and then dried at 40 °C for 1, 3 and 5 days. 1D, 2D and immobile trajectories are shown in red, blue and black, respectively. (b) Relationship between diffusion coefficient (D_{SMT}) and transverse variance (σ_δ^2) obtained from individual 1D trajectories in **Figure 2a**.

Similar results were obtained for other samples, including a PS-*b*-PEO film prepared from its THF solution and dried at 30 °C at different t_{dry} (**Figure 3**). A number of 1D trajectories were observed in **Figure 3a**, and D_{SMT} and σ_δ^2 exhibited wide distributions with no correlation (**Figure 3b**). The diffusion directions reflecting the microdomain orientations were reasonably coherent within μm-scale grains, as reported previously.[36] Importantly, decreases in D_{SMT} and σ_δ^2 at longer

t_{dry} in **Figure 3b** were more noticeable than those in **Figure 2b**, probably reflecting the higher compatibility of THF to PEO as compared with benzene (**Table 1**, *vide infra*).

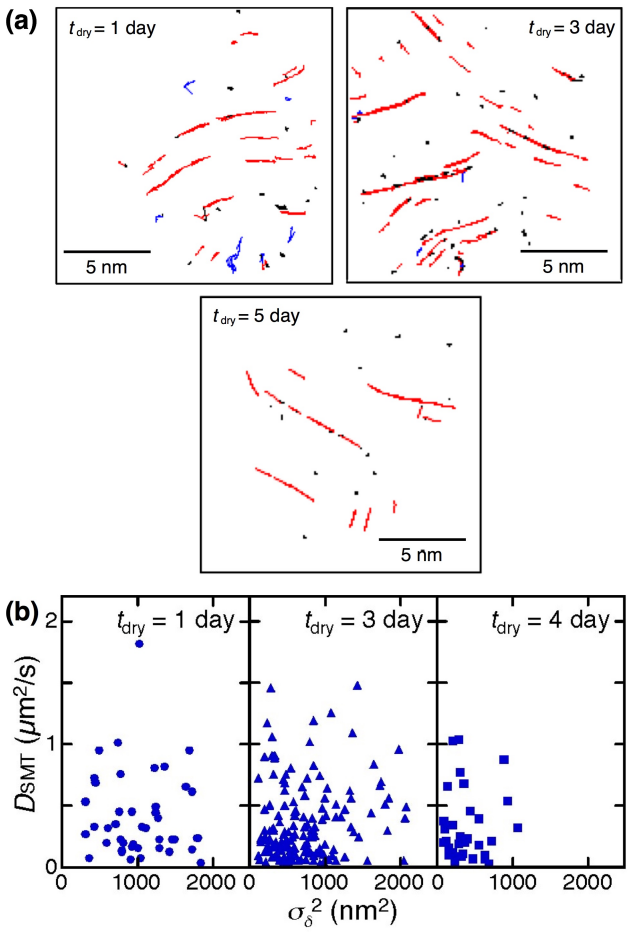

Figure 3. (a) Representative single-molecule trajectories > 10 consecutive frames in length that were measured in a PS-*b*-PEO film prepared from a THF solution (25 wt%) and then dried at 30 °C for 1, 3 and 4 days. 1D, 2D and immobile trajectories are shown in red, blue and black, respectively. (b) Relationship between diffusion coefficient (D_{SMT}) and transverse variance (σ_δ^2) obtained from individual 1D trajectories in **Figure 3a**.

It should be noted that it is inappropriate to compile D_{SMT} and σ_δ^2 values from different videos because the S/N ratios were observed to vary from video to video. Thus, the average of D_{SMT} (D) and effective microdomain radius (r), the latter of which was calculated from the average σ_δ^2 ($\langle\sigma_\delta^2\rangle$) and the average position error of immobile trajectories ($\langle\sigma_{other}^2\rangle$), were

obtained for each video. The effects of solvent evaporation and solvent compatibility on the microdomain properties were discussed based on the average and 80% confidence interval of D and r values obtained at 3-15 different locations in 2-3 different samples (in total, 9-22 videos) prepared under the same conditions.

Figure 4 shows D and r values as a function of t_{dry} measured for PS-*b*-PEO films that were prepared from benzene solutions and dried at different temperatures (30 and 40 °C). At both of the temperatures, D gradually decreased at longer t_{dry} (**Figure 4a**), whereas r decreased in the first two days and changed negligibly thereafter (**Figure 4b**). These changes could be primarily explained by film deswelling induced by solvent evaporation, as supported by the larger change in D observed at the lower drying temperature, with slower solvent evaporation. The larger D and r observed at t_{dry} = 1 day indicate that the films were swollen to a larger extent. Interestingly, evaporation-induced changes in r were similar at these temperatures, possibly reflecting the poor swelling of the PEO microdomains by benzene, as infered by the Hansen solubility parameter (**Table 1**). Since D and r did not change significantly in the 40 °C experiment after t_{dry} = 3 days, SMT measurements for the other solution systems were carried out for t_{dry} = 1 – 4 days.

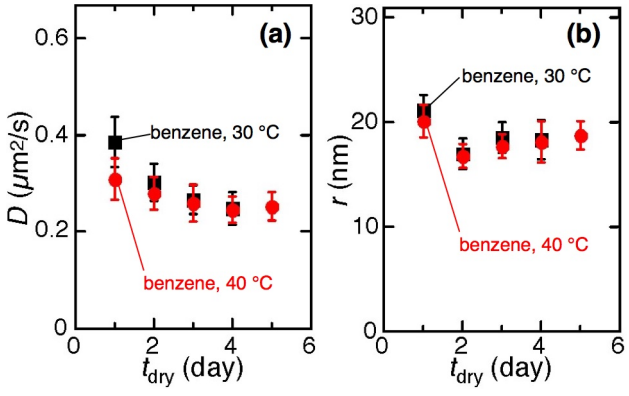

Figure 4. (a) Average 1D diffusion coefficient (D) and (b) effective microdomain radius (r) at different t_{dry} for PS-*b*-PEO films prepared from benzene solutions and dried at 40 °C (red circles) and 30 °C (black squares). These data were calculated from the average values of 9-16 SMT

videos recorded at different locations in 2–3 different PS-*b*-PEO films. The error bars represent the 80% confidence intervals.

Figure 5 shows the effects of MeOH addition (14 wt%) to benzene on the t_{dry}-dependence of D and r. The MeOH addition did not change D significantly, possibly because MeOH evaporated more quickly from the films, as suggested by its lower boiling point (64.7 °C vs. 80.1 °C)[46] and/or the added amount of MeOH was not sufficient to observe any permeability changes. In contrast, slightly smaller r was observed in the presence of MeOH, especially at t_{dry} ≥ 2 days, suggesting that more condensed PEO microdomains were formed as a result of the removal of the PEO-selective solvent. Importantly, the r values at t_{dry} = 2-4 days for the benzene-MeOH samples (14.8–16.0 nm) were close to the value estimated from AFM images of a dried PS-*b*-PEO film (14 ± 2 nm, **Figure S1**). This means that most of the solvents were removed from the PEO microdomains at t_{dry} ≥ 2 days, and the small amount of remaining solvent influenced the microdomain permeability.

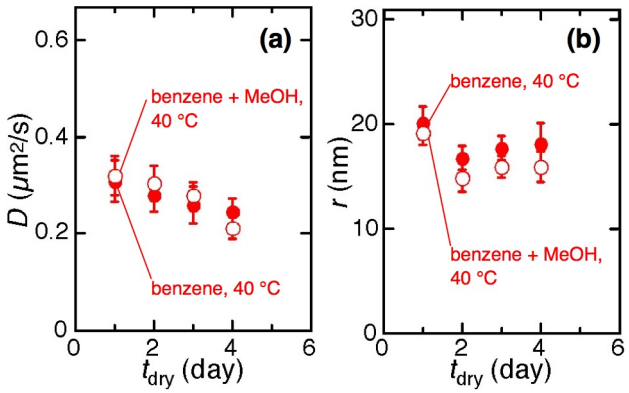

Figure 5. (a) Average 1D diffusion coefficient (D) and (b) effective microdomain radius (r) at different t_{dry} for PS-*b*-PEO films prepared from solutions of 14% methanol in benzene (open red circles) and pure benzene (filled red circles). These data were calculated from the average values of 13-15 SMT videos recorded at different locations in 2–3 different PS-*b*-PEO films. The error bars represent the 80% confidence intervals.

Figure 6 shows the t_{dry}-dependences of D and r for PS-*b*-PEO films that were prepared from benzene and THF solutions and dried at 40 °C and 30 °C, respectively. The different drying temperaures were selected to yield similar evaporation rates for the two solvents of different volatility (boiling points: 80.1 °C vs. 66.0 °C, respectively)[46]. As suggested from **Figures 2b** and **3b**, the PS-*b*-PEO films prepared from THF solutions exhibited larger D at t_{dry} = 1–2 days as compared to those from benzene solutions, indicating that PEO microdomains were better swollen due to their greater compatibility with THF. On the other hand, r was similar in both types of samples, suggesting the presence of a limited amount of residual solvent in the films after drying for more than 1 day.

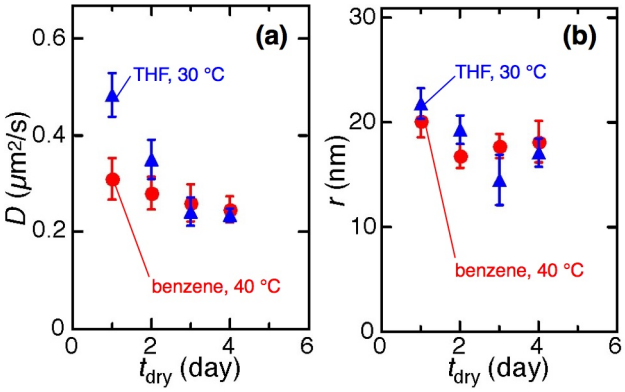

Figure 6. (a) Average 1D diffusion coefficient (D) and (b) effective microdomain radius (r) at different t_{dry} for PS-*b*-PEO films prepared from benzene solutions (red circles) and THF solutions (blue triangles). These data were calculated from the average values of 10-21 SMT videos recorded at different locations in 2–3 different PS-*b*-PEO films. The error bars represent the 80% confidence intervals.

On the other hand, negligible influences of MeOH addition on D and r were observed for PS-*b*-PEO films prepared from THF solutions (**Figure 7**). The concentration of THF in the precursor solutions was approximately 6 times higher than that of MeOH, and thus the PEO microdomains were primarily swollen by THF. In addition, the MeOH/THF ratio in the PEO

microdomains remained appoximately the same during the drying process, due to their similar volatilities, as suggested by their similar boiling points. As a result, the MeOH addition gave negligible influence on the microdomain properties. The plateaued r values at t_{dry} = 3–4 days (14.5–17.2 nm) seemed to be slightly smaller than those for the benzene solutions (**Figure 4b**; 16.7–18.6 nm), suggesting that more condensed PEO microdomains were formed by the evaporation of the PEO-selective solvents as with the benzene-MeOH system (*vide supra*).

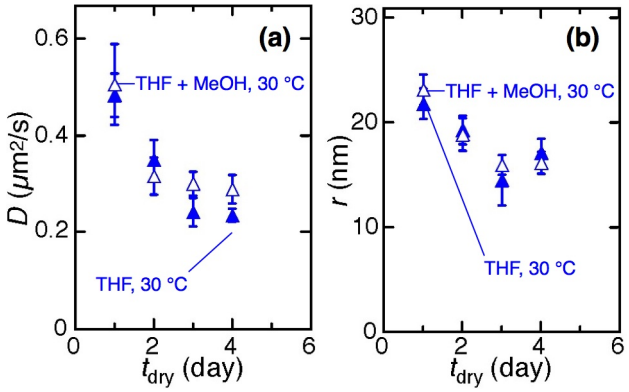

Figure 7. (a) Average 1D diffusion coefficient (D) and (b) effective microdomain radius (r) at different t_{dry} for PS-*b*-PEO films prepared from solutions of 14% methanol in THF (open blue triangles) and pure THF (filled blue triangles). These data were calculated from the average values of 10-22 SMT video data recorded at different locations of 2–3 different PS-*b*-PEO films. The error bars represent the 80% confidence intervals.

Conclusions

This study has shown the applicability of SMT for investigating the properties of cylindrical BCP microdomains in solvent-swollen films. The microdomian permeability and transverse width could be quantitatively assessed by analyzing each of the 1D trajectories originating from the diffusional motions of single SRB molecules. The SMT data revealed the wide distributions of these properties and no evidence of any apparent correlation between their

values, suggesting a nonuniform solvent distribution in the partly dried films. In addition, the SMT measurements offered valuable insights into the roles of solvents in microdomain properties. The presence of residual PEO-swelling solvents enhanced the permeability of PEO microdomains, and also the formation of more condensed PEO microdomains as a result of solvent evaporation. We are exploring the SMT approach for investigating microdomain permeability, morphologies/dimensions and nanoscale environments[50,51] for other cylinder-forming BCPs.

Notes

The authors declare no competing financial interest.

Supporting Information

Wide-field fluorescence videos (**Videos 1-6**) and an AFM image (**Figure S1**) are available free of charge via the Internet at http://pubs.acs.org.

Acknowledgments

The authors gratefully acknowledge the Division of Chemical Sciences, Geosciences, and Biosciences, Office of Basic Energy Sciences of the U.S. Department of Energy (DE-SC0002362) for financial support of this work.

References

(1) Bates, F. S.; Fredrickson, G. H. Block Copolymers - Designer Soft Materials. *Phys. Today* **1999**, *52*, 32-38.
(2) Bates, F. S.; Hillmyer, M. A.; Lodge, T. P.; Bates, C. M.; Delaney, K. T.; Fredrickson, G. H. Multiblock Polymers: Panacea or Pandora's Box? *Science* **2012**, *336*, 434-440.
(3) Park, C.; Yoon, J.; Thomas, E. L. Enabling Nanotechnology with Self Assembled Block Copolymer Patterns. *Polymer* **2003**, *44*, 6725-6760.
(4) Bang, J.; Jeong, U.; Ryu, D. Y.; Russell, T. P.; Hawker, C. J. Block Copolymer Nanolithography: Translation of Molecular Level Control to Nanoscale Patterns. *Adv. Mater.* **2009**, *21*, 4769-4792.
(5) Kim, H.-C.; Park, S.-M.; Hinsberg, W. D. Block Copolymer Based Nanostructures: Materials, Processes, and Applications to Electronics. *Chem. Rev.* **2010**, *110*, 146-177.
(6) Jackson, E. A.; Hillmyer, M. A. Nanoporous Membranes Derived from Block Copolymers: From Drug Delivery to Water Filtration. *ACS Nano* **2010**, *4*, 3548-3553.
(7) Ito, T. Block Copolymer-Derived Monolithic Polymer Films and Membranes Comprising Self-Organized Cylindrical Nanopores for Chemical Sensing and Separations. *Chem.–Asian J.* **2014**, *9*, 2708-2718.
(8) Nunes, S. P. Block Copolymer Membranes for Aqueous Solution Applications. *Macromolecules* **2016**, *49*, 2905-2916.
(9) Hallinan, D. T., Jr.; Balsara, N. P. Polymer Electrolytes. *Annu. Rev. Mater. Res.* **2013**, *43*, 503-525.
(10) Young, W.-S.; Kuan, W.-F.; Epps, T. H., III Block Copolymer Electrolytes for Rechargeable Lithium Batteries. *J. Polym. Sci. B: Polym. Phys.* **2014**, *52*, 1-16.
(11) Darling, S. B. Directing the Self-Assembly of Block Copolymers. *Prog. Polym. Sci.* **2007**, *32*, 1152-1204.
(12) Hamley, I. W. Ordering in Thin Films of Block Copolymers: Fundamentals to Potential Applications. *Prog. Polym. Sci.* **2009**, *34*, 1161-1210.
(13) Sinturel, C.; Vayer, M.; Morris, M.; Hillmyer, M. A. Solvent Vapor Annealing of Block Polymer Thin Films. *Macromolecules* **2013**, *46*, 5399-5415.
(14) Kim, G.; Libera, M. Morphological Development in Solvent-Cast Polystyrene-Polybutadiene-Polystyrene (SBS) Triblock Copolymer Thin Films. *Macromolecules* **1998**, *31*, 2569-2577.
(15) Fukunaga, K.; Elbs, H.; Magerle, R.; Krausch, G. Large-Scale Alignment of ABC Block Copolymer Microdomains via Solvent Vapor Treatment. *Macromolecules* **2000**, *33*, 947-953.
(16) Kim, S. H.; Misner, M. J.; Xu, T.; Kimura, M.; Russell, T. P. Highly Oriented and Ordered Arrays from Block Copolymers via Solvent Evaporation. *Adv. Mater.* **2004**, *16*, 226-231.
(17) Osuji, C. O. Alignment of Self-Assembled Structures in Block Copolymer Films by Solvent Vapor Permeation. *Macromolecules* **2010**, *43*, 3132-3135.
(18) Tran-Ba, K.-H.; Finley, J. J.; Higgins, D. A.; Ito, T. Single-Molecule Tracking Studies of Millimeter-Scale Cylindrical Domain Alignment in Polystyrene-Poly(ethylene oxide) Diblock Copolymer Films Induced by Solvent Vapor Penetration. *J. Phys. Chem. Lett.* **2012**, *3*, 1968-1973.
(19) Li, Y.; Huang, H.; He, T.; Gong, Y. The Effect of the Preferential Affinity of the Solvent on the Microstructure of Solution-Cast Block Copolymer Thin Films. *J. Phys. Chem. B*

2010, *114*, 1264-1270.
(20) Kim, B.; Hong, S. W.; Park, S.; Xu, J.; Hong, S.-K.; Russell, T. P. Phase Transition Behavior in Thin Films of Block Copolymers by Use of Immiscible Solvent Vapors. *Soft Matter* **2011**, *7*, 443-447.
(21) Park, W. I.; Choi, Y. J.; Yun, J. M.; Hong, S. W.; Jung, Y. S.; Kim, K. H. Enhancing the Directed Self-assembly Kinetics of Block Copolymers Using Binary Solvent Mixtures. *ACS Appl. Mater. Interfaces* **2015**, *7*, 25843-25850.
(22) Tsukruk, V. V. Scanning Probe Microscopy of Polymer Surfaces. *Rubber Chem. Technol.* **1997**, *70*, 430-467.
(23) Ito, T.; Grabowska, I.; Ibrahim, S. Chemical-Force Microscopy for Materials Characterization. *Trends Anal. Chem.* **2010**, *29*, 225-233.
(24) Jinnai, H.; Spontak, R. J.; Nishi, T. Transmission Electron Microtomography and Polymer Nanostructures. *Macromolecules* **2010**, *43*, 1675-1688.
(25) Papadakis, C. M.; Di, Z.; Posselt, D.; Smilgies, D.-M. Structural Instabilities in Lamellar Diblock Copolymer Thin Films During Solvent Vapor Uptake. *Langmuir* **2008**, *24*, 13815-13818.
(26) Paik, M. Y.; Bosworth, J. K.; Smilges, D.-M.; Schwartz, E. L.; Andre, X.; Ober, C. K. Reversible Morphology Control in Block Copolymer Films via Solvent Vapor Processing: An in Situ GISAXS Study. *Macromolecules* **2010**, *43*, 4253-4260.
(27) Bai, W.; Yager, K. G.; Ross, C. A. In Situ Characterization of the Self-Assembly of a Polystyrene-Polydimethylsiloxane Block Copolymer during Solvent Vapor Annealing. *Macromolecules* **2015**, *48*, 8574-8584.
(28) Gu, X.; Gunkel, I.; Hexemer, A.; Russell, T. P. Controlling Domain Spacing and Grain Size in Cylindrical Block Copolymer Thin Films by Means of Thermal and Solvent Vapor Annealing. *Macromolecules* **2016**, *49*, 3373-3381.
(29) Paradiso, S. P.; Delaney, K. T.; Garcia-Cervera, C. J.; Ceniceros, H. D.; Fredrickson, G. H. Block Copolymer Self Assembly during Rapid Solvent Evaporation: Insights into Cylinder Growth and Stability. *ACS Macro Lett.* **2014**, *3*, 16-20.
(30) Paradiso, S. P.; Delaney, K. T.; Garcia-Cervera, C. J.; Ceniceros, H. D.; Fredrickson, G. H. Cyclic Solvent Annealing Improves Feature Orientation in Block Copolymer Thin Films. *Macromolecules* **2016**, *49*, 1743-1751.
(31) Moerner, W. E.; Fromm, D. P. Methods of Single-Molecule Fluorescence Spectroscopy and Microscopy. *Rev. Sci. Instrum.* **2003**, *74*, 3597-3619.
(32) Michaelis, J.; Brauchle, C. Reporters in the Nanoworld: Diffusion of Single Molecules in Mesoporous Materials. *Chem. Soc. Rev.* **2010**, *39*, 4731-4740.
(33) Lebold, T.; Michaelis, J.; Brauchle, C. The Complexity of Mesoporous Silica Nanomaterials Unravelled by Single Molecule Microscopy. *Phys. Chem. Chem. Phys.* **2011**, *13*, 5017-5033.
(34) Higgins, D. A.; Tran-Ba, K.-H.; Ito, T. Following Single Molecules to a Better Understanding of Self-Assembled One-Dimensional Nanostructures. *J. Phys. Chem. Lett.* **2013**, *4*, 3095-3103.
(35) Higgins, D. A.; Park, S. C.; Tran-Ba, K.-H.; Ito, T. Single-Molecule Investigations of Morphology and Mass Transport Dynamics in Nanostructured Materials. *Annu. Rev. Anal. Chem.* **2015**, *8*, 193-216.
(36) Tran-Ba, K.-H.; Higgins, D. A.; Ito, T. Single-Molecule Tracking Studies of Flow-Induced Microdomain Alignment in Cylinder-Forming Polystyrene-Poly(ethylene oxide) Diblock

Copolymer Films. *J. Phys. Chem. B* **2014**, *118*, 11406-11415.
(37) Tran Ba, K. H.; Everett, T. A.; Ito, T.; Higgins, D. A. Trajectory Angle Determination in One Dimensional Single Molecule Tracking Data by Orthogonal Regression Analysis. *Phys. Chem. Chem. Phys.* **2011**, *13*, 1827-1835.
(38) Tran-Ba, K.-H.; Higgins, D. A.; Ito, T. Fluorescence Recovery after Photobleaching and Single-Molecule Tracking Measurements of Anisotropic Diffusion within Identical Regions of a Cylinder-Forming Diblock Copolymer Film. *Anal. Chem.* **2015**, *87*, 5802-5809.
(39) Xu, J.; Hong, S. W.; Gu, W.; Lee, K. Y.; Kuo, D. S.; Xiao, S.; Russell, T. P. Fabrication of Silicon Oxide Nanodots with an Areal Density Beyond 1 Teradots $Inch^{-2}$. *Adv. Mater.* **2011**, *23*, 5755-5761.
(40) Kim, D. H.; Jia, X.; Lin, Z.; Guarini, K. W.; Russell, T. P. Growth of Silicon Oxide in Thin Film Block Copolymer Scaffolds. *Adv. Mater.* **2004**, *16*, 702-706.
(41) Mao, H.; Hillmyer, M. A. Nanoporous Polystyrene by Chemical Etching of Poly(ethylene oxide) from Ordered Block Copolymers. *Macromolecules* **2005**, *38*, 4038-4039.
(42) Hahn, J.; Filiz, V.; Rangou, S.; Clodt, J.; Jung, A.; Buhr, K.; Abetz, C.; Abetz, V. Structure Formation of Integral-Asymmetric Membranes of Polystyrene-*block*-Poly(ethylene oxide). *J. Polym. Sci. B: Polym. Phys.* **2013**, *51*, 281-290.
(43) Karunakaran, M.; Nunes, S. P.; Qiu, X.; Yu, H.; Peinemann, K.-V. Isoporous PS-*b*-PEO Ultrafiltration Membranes via Self-Assembly and Water-Induced Phase Separation. *J. Membr. Sci.* **2014**, *453*, 471-477.
(44) Hansen, C. M.: *Hansen Solubility Parameters: A User's Handbook*; CRC Press: Boca Raton, 2000.
(45) Hansen Solubility Parameters. http://www.hansen-solubility.com/ (accessed October 9 2016).
(46) Speight, J. G.: *Lange's Handbook of Chemistry, 16th Ed.*; McGrow-Hill: New York, 2005.
(47) Wang, C.; Yang, S.; Xu, J.; Zhu, M. Morphology Transformation of Polystyrene-*block*-Poly(ethylene oxide) Vesicle on Surface. *Polymer* **2013**, *54*, 3709-3715.
(48) Ratner, M. A.; Shriver, D. F. Ion-Transport in Solvent-Free Polymers. *Chem. Rev.* **1988**, *88*, 109-124.
(49) Deen, W. M. Hindered Transport of Large Molecules in Liquid-Filled Pores. *AIChE J.* **1987**, *33*, 1409-1425.
(50) Giri, D.; Hanks, C. N.; Collinson, M. M.; Higgins, D. A. Single-Molecule Spectroscopic Imaging Studies of Polarity Gradients Prepared by Infusion-Withdrawal Dip-Coating. *J. Phys. Chem. C* **2014**, *118*, 6423-6432.
(51) Kumarasinghe, R.; Higgins, E. D.; Ito, T.; Higgins, D. A. Spectroscopic and Polarization-Dependent Single-Molecule Tracking Reveal the One-Dimensional Diffusion Pathways in Surfactant-Templated Mesoporous Silica. *J. Phys. Chem. C* **2016**, *120*, 715-723.

Table of Contents Only

Single-Molecule Tracking Study of the Permeability and Transverse Width of Individual Cylindrical Microdomains in Solvent-Swollen Polystyrene-*block*-Poly(ethylene oxide) Films

Dol Raj Sapkota, Khanh-Hoa Tran-Ba,† Trevor Elwell-Cuddy, Daniel A. Higgins,* and Takashi Ito*